Applications of a Variational Multiscale Method for Large Eddy Simulation of Turbulent Flows on Moving/Deforming Unstructured Grids

Ajaykumar Rajasekharan [a] and Charbel Farhat [a]

[a] *Department of Mechanical Engineering, Stanford University, Stanford, CA 94305-3035, USA*

Abstract

In this paper the three level formulation of a variational multiscale (VMS) large eddy simulation (LES) method for compressible flow computations [5,6] is extended for applications involving moving/deforming grids. A consistent method to improve the VMS-LES method by computing the small-scale Smagorinsky constant ($\mathcal{C}_s'$) dynamically [6, 19] as the flow develops (dynamic VMS-LES) is also extended for dynamic grid applications. Two applications of VMS-LES for the simulation of separated flow over moving NACA-0012 extruded airfoil is then presented. The first application involves a qualitative simulation exploring the Knoller-Betz effect [38] of the heaving airfoil at high Strouhal number. The second application is that of the pitching airfoil undergoing dynamic stall. The results predicted by the dynamic VMS-LES method are compared to those obtained with other turbulence models and to experimental data and it is found that the dynamic VMS-LES performs better than the other considered static and dynamic LES models.

Key words: agglomeration, compressible turbulent flows, dynamic LES, unstructured meshes, variational Germano's identity, variational multiscale

1 Introduction

Since its introduction in [1–3] the VMS-LES method has been successfully applied to simulate many practically relevant turbulent flow computations. In this approach the Navier-Stokes (NS) equations are treated by a variational

[1] Corresponding author; e-mail: rajay@stanfordalumni.org

projection instead of the classical filtering methodology. As clarified later in [4], in VMS-LES, spatial scales are separated *a priori* and a system of equations, each representing the dynamics of one of the separated scales, are derived. Thus, this formalism offers the freedom to choose different closure models for equations representing different scales. The system of equations can then be recombined to obtain the final variational form of the NS equations appended with closure models. Typically in VMS-LES, the effect of the unresolved scales is modeled only in the equations representing the smallest resolved scales. Therefore, no energy is directly extracted from the large structures in the flow. These class of methods have shown great promise in simulation of different turbulent flows, such as wall bounded flows [3], separated turbulent flows [5–7], turbulent flow control [8] and simulation of bypass transition [9] to name a few.

Many variants of the VMS-LES method have been developed over the last few years. Initial attention focused on incompressible flows, regular grids and spectral discretizations wherein the *a priori* separation of scales was achieved via a frequency cutoff [1–3]. For finite element approximations, a scale separation algorithm based on hierarchical bases was presented in [10]. For compressible turbulent flows, a more general approach for discretizing the the two-level VMS-LES formulation on unstructured finite volume (FV) as well as finite element (FE) meshes was proposed in [5]. Later in [6] a three-level formalism in tandem to the approach in [4] for incompressible flows was derived and was shown to introduce requirement of closure terms in the continuity equation as-well.

VMS-LES involves two stages, first is a formalism stage as described in the first two paragraphs and the second is a closure stage. In most previous works on the VMS-LES method, the closure was achieved by extracting energy from the small resolved scales by the Smagorinsky eddy viscosity model with a constant coefficient [11]. In [12], a dynamic VMS-LES method was constructed by computing this coefficient dynamically using the same procedure as in the original dynamic subgrid-scale eddy viscosity model [13]. In that study, it was concluded that the dynamic multiscale model was less sensitive to the scale partition when compared to its static counterpart. In [14], an iterative procedure based on the concept of residual-free bubbles [15] was proposed for adjusting dynamically the value of the coefficient of the Smagorinsky eddy viscosity model. An alternative approach for constructing a dynamic VMS-LES method that is based on a simple variational interpretation of Germano's identity [16,17] was proposed in [6]. The salient features of this alternative approach are numerous. They include: (a) consistency with the variational aspect of the VMS-LES method as opposed to the straightforward procedure adopted in [12] for incorporating a dynamic subgrid-scale eddy viscosity model, (b) consistency of the value of the dynamically computed Smagorinsky constant with the adopted discretization method (similar to the vector-level identity

presented in [16, 18]), and (c) incorporation of the time-history and diffusive effects by incorporation of the inertial and viscous terms in the computation of the dynamic Smagorinsky constant.

With the increase in computational power over the years, and the development of near wall models, it is now feasible to apply LES simulations to study flow over small sized fixed and flapping wings in the low to moderate speed aerodynamics regime. This development has opened up an opportunity to successfully study flow over Micro Air Vehicles (MAV). It is thus worthwhile in exploring the efficacy of the VMS-LES method in capturing the such unsteady aerodynamic flows over moving boundaries. This paper is hence an attempt to study the applicability of the VMS-LES method for flows on moving and deforming grids. In this respect, this paper is essentially a sequel to the previous works done in [5–7].

This paper is organized as follows. Section 2 summarizes the arbitrary Lagrangian-Eulerian (ALE) governing equations and the FV/FE formulation. Section 3 describes the VMS-LES formulation of compressible turbulent flows developed in [5] and re-derived in [6]. In particular, its agglomeration-based procedure for separating *a priori* the scales on unstructured meshes is highlighted. In Section 4, an overview of a dynamic extension of the VMS-LES based on the variational interpretation of Germano's identity [6, 16] is presented. Next in Section 5, the specifics of the spatial and temporal discretizations adopted in this work are discussed. In Section 6, the results from the application of the dynamic VMS-LES method to the simulation a heaving and pitching extruded NACA-0012 airfoil is presented and the results are discussed. Finally, Section 7 concludes this paper with a summary of the findings and reflections on future improvements and challenges.

2 Arbitrary Lagrangian-Eulerian (ALE) formulation of the governing equations and its semi-discretization

Let $\Omega(\mathbf{x}, t)$ be the flow domain of interest and $\Gamma(t)$ be its moving and/or deforming boundary. Also let the mapping function between instantaneous configuration $\Omega(\mathbf{x}, t)$ (where coordinates in space is denoted by $\mathbf{x}$ and time is denoted by t) and the reference configuration $\Omega(\xi, 0)$ (where coordinates in space is denoted by ξ and time is denoted by τ) be represented as $\mathbf{x} = \mathbf{x}(\xi, \tau)$ with $t = \tau$. Then the ALE strong conservation form of set of mass, momentum

and energy equations governing a compressible fluid can be written down as

$$\begin{cases} \dfrac{\partial(J\rho)}{\partial t} + J\nabla.(\rho(\mathbf{u}-\mathbf{w})) & = 0 \\ \dfrac{\partial(J\rho\mathbf{u})}{\partial t} + J\nabla.(\rho\mathbf{u}\otimes(\mathbf{u}-\mathbf{w})) & = -\nabla P + \nabla.\boldsymbol{\sigma} \\ \dfrac{\partial(JE)}{\partial t} + J\nabla.[(E(\mathbf{u}-\mathbf{w}) + P\mathbf{u})] & = \nabla.(\boldsymbol{\sigma}\mathbf{u}) + \nabla.(\lambda\nabla T) \end{cases} \tag{1}$$

where ρ is the density, $\mathbf{u}$ is the velocity, P is the pressure, $\boldsymbol{\sigma}$ is the viscous stress tensor, E is the total energy, λ is the thermal conductivity, and T is the temperature of the fluid. The viscous stress tensor is given by $\boldsymbol{\sigma}_{ij} = \mu(2\mathbf{S}_{ij} - \frac{2}{3}\mathbf{S}_{kk}\delta_{ij})$ where μ denotes the viscosity, $\mathbf{S}_{ij} = \frac{1}{2}(\frac{\partial \mathbf{u}_i}{\partial \mathbf{x}_j} + \frac{\partial \mathbf{u}_j}{\partial \mathbf{x}_i})$, $\mathbf{x}$ denotes the position vector, $J = det\left(\frac{d\mathbf{x}}{d\xi}\right)$ and $\mathbf{w}$ denotes the mesh velocity. The total energy E is given by $E = \rho C_v T + \frac{1}{2}\rho\mathbf{u}.\mathbf{u}$ where C_v is the specific heat at constant volume, and ρ, P, and T are assumed to satisfy the state equation for a perfect gas — that is, $P = \rho RT$. The kinematic viscosity μ and thermal conductivity λ are assumed to be constant.

Without any loss of generality as far as issues pertaining to unstructured meshes, the following spatial discretization is assumed:

- The bounded flow domain Ω is discretized by a tetrahedral mesh from which a dual mesh defined by cells or control volumes is derived.
- The convective fluxes are approximated by a finite volume (FV) method in which $\mathcal{X}_i$ denotes the characteristic function corresponding to the control volume C_i associated with node i.
- The diffusive fluxes are approximated by a piecewise linear finite element (FE) method in which Φ_i denotes the P1 shape function associated with node i.

Now, integrating Eq. (1) on an elementary volume of the material/reference (ξ) space and transforming back to the physical ($\mathbf{x}$) space, the following mixed FE/FV formulation is obtained

$$\begin{cases} A(\mathcal{X}_i, \mathbf{W}, \mathbf{w}) & = 0 \\ \mathbf{B}(\mathcal{X}_i, \Phi_i, \mathbf{W}, \mathbf{w}) & = \mathbf{0} \\ C(\mathcal{X}_i, \Phi_i, \mathbf{W}, \mathbf{w}) & = 0 \end{cases} \tag{2}$$

where $\mathbf{W} = (\rho, \mathbf{u}, T)^t$ and

$$\begin{cases} A(\mathcal{X}_i, \mathbf{W}, \mathbf{w}) & = \int_{\Omega(t)} \dfrac{\partial \rho}{\partial t} \mathcal{X}_i \, d\Omega \; + \; \int_{\partial\Omega_i(t)} \rho(\mathbf{u} - \mathbf{w}).\mathbf{n}\mathcal{X}_i \, d\Gamma \\ \mathbf{B}(\mathcal{X}_i, \Phi_i, \mathbf{W}, \mathbf{w}) & = \int_{\Omega(t)} \dfrac{\partial \rho \mathbf{u}}{\partial t} \mathcal{X}_i \, d\Omega \; + \; \int_{\partial\Omega_i(t)} \rho \, \mathbf{u} \otimes (\mathbf{u} - \mathbf{w}) \, \mathbf{n}\mathcal{X}_i \, d\Gamma \\ & \quad + \int_{\partial\Omega_i(t)} P\mathbf{n}\mathcal{X}_i \, d\Gamma \; + \; \int_{\Omega(t)} \boldsymbol{\sigma} \nabla \Phi_i d\Omega \\ C(\mathcal{X}_i, \Phi_i, \mathbf{W}, \mathbf{w}) & = \int_{\Omega(t)} \dfrac{\partial E}{\partial t} \mathcal{X}_i \, d\Omega \; + \; \int_{\partial\Omega_i(t)} (E(\mathbf{u} - \mathbf{w}) + P\mathbf{u}).\mathbf{n}\mathcal{X}_i \, d\Gamma \\ & \quad + \int_{\Omega(t)} \boldsymbol{\sigma}\mathbf{u}.\nabla\Phi_i \, d\Omega \; + \; \int_{\Omega(t)} \lambda \nabla T.\nabla \Phi_i \, d\Omega \end{cases} \tag{3}$$

In the above equations, $\partial\Omega_i(t)$ denotes the boundary of the support of $\mathcal{X}_i$, $\mathbf{n}$ the outward normal to this support, and a component of $\mathbf{W}$ is semi-discretized by a FV approach when appearing in an integral containing $\mathcal{X}_i$ and by a FE approach when appearing in an integral containing Φ_i.

3 VMS-LES formulation of the ALE governing equations

Let $\mathcal{V}_{FV}$ and $\mathcal{V}_{FE}$ denote the spaces spanned by the characteristic functions $\{\mathcal{X}_k\}$ and the shape functions $\{\Phi_k\}$, respectively. The decomposition *a* priori of these spaces into large resolved scales, small resolved scales, and unresolved scales (a.l.a. Collis [4]) can be written as

$$\mathcal{V}_{FV} = \overline{\mathcal{V}}_{FV} \oplus \mathcal{V}'_{FV} \oplus \widehat{\mathcal{V}}_{FV} \tag{4}$$

and

$$\mathcal{V}_{FE} = \overline{\mathcal{V}}_{FE} \oplus \mathcal{V}'_{FE} \oplus \widehat{\mathcal{V}}_{FE} \tag{5}$$

where the notation "$-$", "$\prime$", and "$\wedge$" designates the large resolved, small resolved, and unresolved scales,

Plugging these decompositions in Eq. (3) a coupled set of equations for large, small and unresolved scales are obtained [6, 7]. Neglecting the effect of unresolved scales on large scales and recombining the large and small scale equa-

tions the following set of discretized (subscript $'h'$) equations is achieved

$$\begin{cases} A(\mathcal{X}_{i_h}, \mathbf{W}_h, \mathbf{w}) \ + \ A'(\mathcal{X}'_i, \mathbf{W}', \widehat{\mathbf{W}}, \mathbf{w}) \ + \ R_c(\mathcal{X}'_i, \widehat{\mathbf{W}}, \mathbf{w}) \\ \quad + \ C_c(\mathcal{X}'_i, \overline{\mathbf{W}}, \widehat{\mathbf{W}}, \mathbf{w}) & = 0 \\ \mathbf{B}(\mathcal{X}_{i_h}, \Phi_{i_h}, \mathbf{W}_h i, \mathbf{w}) \ + \ \mathbf{B}'(\mathcal{X}'_i, \Phi'_i, \mathbf{W}', \widehat{\mathbf{W}}, \mathbf{w}) + \mathbf{R}_m(\mathcal{X}'_i, \widehat{\mathbf{W}}, \mathbf{w}) \\ \quad + \ \mathbf{C}_m(\mathcal{X}'_i, \Phi'_i, \overline{\mathbf{W}}, \widehat{\mathbf{W}}, \mathbf{w}) & = \mathbf{0} \\ C(\mathcal{X}_{i_h}, \Phi_{i_h}, \mathbf{W}_h) \ + \ C'(\mathcal{X}'_i, \Phi'_i, \mathbf{W}', \widehat{\mathbf{W}}, \mathbf{w}) + R_e(\mathcal{X}'_i, \Phi'_i, \widehat{\mathbf{W}}, \mathbf{w}) \\ \quad + \ C_e(\mathcal{X}'_i, \Phi'_i, \overline{\mathbf{W}}, \widehat{\mathbf{W}}, \mathbf{w}) & = 0 \end{cases} \tag{6}$$

where it is noted that unlike the Favre-averaged formulation of the governing equations, the continuity equations requires modeling. Choosing to ignore this modeling, and applying Smagorinsky type closures [11] yields

$$\begin{cases} A(\mathcal{X}_{i_h}, \mathbf{W}_h, \mathbf{w}) & = 0 \\ \mathbf{B}(\mathcal{X}_{i_h}, \Phi_{i_h}, \mathbf{W}_h, \mathbf{w}) \ + \ \mathbf{M}_S\Big(\Phi'_{i_h}, \mathbf{W}'_h, (\mathcal{C}'_s \triangle'_h)^2\Big) & = \mathbf{0} \\ C(\mathcal{X}_{i_h}, \Phi_{i_h}, \mathbf{W}_h, \mathbf{w}) \ + \ M_H\Big(\Phi'_{i_h}, \mathbf{W}'_h, (\mathcal{C}'_s \triangle'_h)^2, Pr_t\Big) & = 0 \end{cases} \tag{7}$$

with,

$$\begin{aligned} \mathbf{M}_S\Big(\Phi'_i, \mathbf{W}', (\mathcal{C}'_s \triangle'_l)^2\Big) \qquad &= \int_\Omega \overline{\rho}(\mathcal{C}'_s \triangle'_l)^2 |\mathbf{S}'| (2\mathbf{S}'_{ij} - \frac{2}{3}\mathbf{S}'_{kk}\delta_{ij}) \nabla \Phi'_i d\Omega \\ M_H\Big(\Phi'_i, \mathbf{W}', (\mathcal{C}'_s \triangle'_l)^2, Pr_t\Big) &= \int_\Omega \frac{C_p \overline{\rho}(\mathcal{C}'_s \triangle'_l)^2 |\mathbf{S}'|}{Pr_t} \nabla T' . \nabla \Phi'_i d\Omega \end{aligned} \tag{8}$$

3.1 A priori Separation of the Scales on Unstructured Entities

A priori separation of the scales according to $\mathcal{V}_{FE/FV_h} = \overline{\mathcal{V}}_{FE/FV_h} \oplus \mathcal{V}'_{FE/FV_h}$ is achieved here by defining a projection operator $\mathcal{P}_h$ such that $\overline{\mathbf{W}}_h = \mathcal{P}_h \mathbf{W}_h$. For this, control volumes and their neighbors in the dual mesh are agglomerated to form macro-cells. Then, as proposed in [5], the large-scale component is

$$\overline{\mathbf{W}}_h = \sum_k \Phi_{k_h} \widetilde{\mathbf{W}}_{k_h} = \sum_k \Phi_{k_h} \left(\frac{\sum\limits_{j \in I_k} Vol(C_j) \mathbf{W}_{j_h}}{\sum\limits_{j \in I_k} Vol(C_j)} \right) = \sum_k \overline{\Phi}_{k_h} \mathbf{W}_{k_h} \tag{9}$$

where C_j denotes the cell around the node j, $Vol(C_j)$ its volume, I_k =

$\{j \ / \ C_j \subset C_{m(k)}\}$, $C_{m(k)}$ the macro-cell containing the cell C_k, and

$$\overline{\Phi}_{k_h} = \frac{Vol(C_k)}{\sum\limits_{j \in I_k} Vol(C_j)} \sum_{j \in I_k} \Phi_{j_h} \tag{10}$$

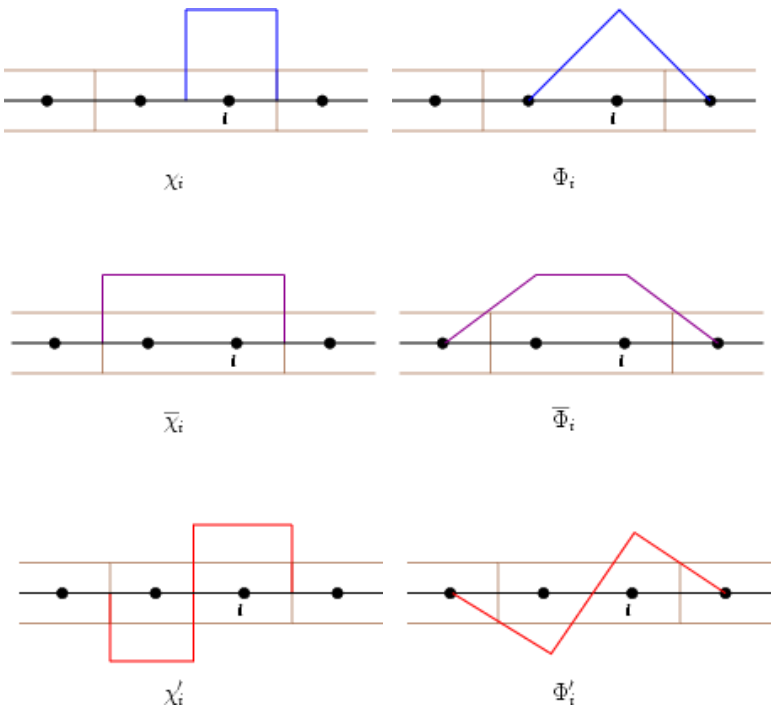

Fig. 1. (left) Coarse scale $\overline{\mathcal{X}}_i$ (Scaling function) and fine scale $\mathcal{X}'_i$ (Haar wavelet) and (right) coarse scale $\overline{\Phi}_i$ (Scaling function) and fine scale Φ'_i (Wavelet)

Remark It is illustrative to note that $\overline{\Phi}_{k_h}$ and $\overline{\mathbf{W}}_h$ represent scaling functions and Φ'_i and $\mathcal{X}'_i$ the corresponding wavelets in the multi-resolution theory of wavelets [22]. In particular $\mathcal{X}'_i$ is none other than the Haar wavelet basis function (see Fig. 1)

3.2 Wall Boundary Treatments of Large and Small Scale Variables

A priori separation of scales also raises the question of which boundary conditions to prescribe for the large and small resolved scales. This issue is addressed here by requiring that the large resolved scales satisfy the no-slip (Dirichlet) boundary conditions and by allowing the small scales to vanish at the wall [21]. This is consistent with the observation that the small eddies (fluctuations) disappear at the wall. Hence, the following boundary restriction is incorporated

into the definition of the large and small resolved scales

$$\begin{cases} \overline{\mathcal{V}}_{FV_h/FE_h} = \{\overline{v}_h : \overline{v}_h = \sum\limits_k \overline{\Phi}_{k_h} v_{k_h}, \overline{\mathbf{u}}_h|_{\Gamma_{wall}} = \mathbf{u}|_{\Gamma_{wall}}\} \\ \mathcal{V}'_{FV_h/FE_h} = \{v'_h = \sum\limits_k (\Phi_{k_h} - \overline{\Phi}_{k_h}) v_{k_h}, \mathbf{u}'_h|_{\Gamma_{wall}} = 0\} \end{cases} \tag{11}$$

The above no-slip condition is enforced naturally by choosing not to agglomerate the first layer of control volumes adjacent to the wall. This approach avoids discontinuities of the large scale velocities at the wall in comparison to strongly prescribing the no-slip conditions [23]. In this way the Gibbs phenomenon [24] is averted.

Remark It should also be mentioned that for computations involving wall-functions (as in moderate to high Reynolds number computations presented in this paper), the VMS-LES approach does not need any extra treatments at the displaced wall boundary. This is because, the wall-function introduces a Dirichlet-to-Neumann transformation which results in imposing a Neumann boundary condition at the displaced boundary.

4 Dynamic Extensions of the Variational Multiscale Method

In the previous section a static VMS-LES formulation [1] for simulation of compressible turbulent flows was presented. One of short comes of this approach is that the Smagorinsky constant $\mathcal{C}'_s$ is constant. Hence, as it is, this static form of the VMS-LES model is not adaptable to the different flow features in the domain. Also this method generates turbulent viscosity even in the laminar regions of the flow domain. To overcome this shortfalls, dynamic versions of the VMS-LES method have been put forth [6, 12]. This section briefly describes the problem statement in developing dynamic LES models and then summarizes the residual based dynamic procedure in [6].

4.1 Problem statement

The procedure to develop a dynamic coefficient version of an LES model can be viewed as a model based parameter estimation problem as shown below

$$\mathcal{C}^{n+1} = \mathbb{E}[\mathcal{C}|\mathbf{W}^n, \mathbf{W}^{n-1}, \mathbf{W}^{n-2}.....] \tag{12}$$

where, the Smagorinsky constant $\mathcal{C}$ is the parameter to be estimated when the small scale eddy viscosity model of Smagorinsky is used to close the equations and $\mathbb{E}$ is the expectation operator.

The classical approach (as in Germano's model [13]) has been to assume a Markovian system, where by the value of $\mathcal{C}^{n+1}$ is assumed to be dependent only on the previous state $\mathbf{W}^n$ i.e.

$$\mathcal{C}^{n+1} = \mathbb{E}[\mathcal{C}|\mathbf{W}^n] \tag{13}$$

The initial attempts to develop a dynamic VMS-LES model in the lines of Germano's approach was done in [12] for incompressible flows, that can be readily extended to compressible flows in the Favre averaged setting. In this section another approach based on the variational analogue of Germano's identity developed in [6] is summarized.

4.2 A residual based dynamic VMS-LES model based on the variational analogue of Germano's identity

Consider two *nested* meshes $\mathbb{M}_1$ and $\mathbb{M}_2$ with element sizes h_1 and $h_2 > h_1$, respectively, and corresponding finite dimensional subspaces $\mathcal{V}_{FV_{h_2}} \subset \mathcal{V}_{FV_{h_1}}$ and $\mathcal{V}_{FE_{h_2}} \subset \mathcal{V}_{FE_{h_1}}$. Also let $\mathcal{C}' = \mathcal{C}_s'^2$ (and $\mathcal{C} = \mathcal{C}_s^2$). Substituting h by h_1 in the second and third of Eqs. (6) the momentum and continuity equations for each node i is obtained. Similarly, discretizing Eqs. (6) on the coarser mesh $\mathbb{M}_2$, but using the prolongated functions ($\mathcal{X}_{i_{h_{2,1}}} = \mathcal{I}_1(\mathcal{X}_{i_{h_2}})$, $\Phi_{i_{h_{2,1}}} = \mathcal{I}_1(\Phi_{i_{h_2}})$, $\mathbf{W}_{h_{2,1}} = \mathcal{I}_1(\mathbf{W}_{h_2})$) and their associated nodal values on $\mathbb{M}_1$ the corresponding momentum and continuity equations for each node i is obtained. Subtracting the first of this equations from the second and defining $\triangle_l' = \triangle_{h_1}'$ yields

$$\begin{cases} \mathbf{B}(\mathcal{X}_{i_{h_{2,1}}}, \Phi_{i_{h_{2,1}}}, \mathbf{W}_{h_{2,1}}, \mathbf{w}) - \mathbf{B}(\mathcal{X}_{i_{h_1}}, \Phi_{i_{h_1}}, \mathbf{W}_{h_1}, \mathbf{w}) \\ \quad = \mathbf{M}_S\Big(\Phi'_{i_{h_1}}, \mathbf{W}'_{h_1}, \mathcal{C}'\triangle_l'^2\Big) - \mathbf{M}_S\Big(\Phi'_{i_{h_{2,1}}}, \mathbf{W}'_{h_{2,1}}, (\frac{\triangle'_{h_2}}{\triangle'_{h_1}})^2\mathcal{C}'\triangle_l'^2\Big) \\ C(\mathcal{X}_{i_{h_{2,1}}}, \Phi_{i_{h_{2,1}}}, \mathbf{W}_{h_{2,1}}, \mathbf{w}) - C(\mathcal{X}_{i_{h_1}}, \Phi_{i_{h_1}}, \mathbf{W}_{h_1}, \mathbf{w}) \\ = M_H\Big(\Phi'_{i_{h_1}}, \mathbf{W}'_{h_1}, \mathcal{C}'\triangle_l'^2, Pr_t\Big) - M_H\Big(\Phi'_{i_{h_{2,1}}}, \mathbf{W}'_{h_{2,1}}, (\frac{\triangle'_{h_2}}{\triangle'_{h_1}})^2\mathcal{C}'\triangle_l'^2, Pr_t\Big) \end{cases} \tag{14}$$

The above two equations relate the resolved turbulent scales to the subgrid-scales at two different levels. Hence, they can be interpreted as a variational form of Germano's identity [13, 16], from which the parameters $\mathcal{C}'\triangle_l'^2$ and Pr_t can be dynamically computed. Choosing subspaces $\mathcal{V}_{FV_{h_2}} = \overline{\mathcal{V}}_{FV_{h_1}}$ and $\mathcal{V}_{FE_{h_2}} = \overline{\mathcal{V}}_{FE_{h_1}}$ the following decomposition is employed

$$\mathcal{V}_{FV/FE_{h_2}} = \overline{\mathcal{V}}_{FV/FE_{h_2}} \oplus \mathcal{V}'_{FV/FE_{h_2}} = \overline{\overline{\mathcal{V}}}_{FV/FE_{h_1}} \oplus \Big[\overline{\mathcal{V}}\Big]'_{FV/FE_{h_1}} \tag{15}$$

Subspaces $\overline{\overline{\mathcal{V}}}_{FE/FV_{h_1}}$ and $\left[\overline{\mathcal{V}}\right]'_{FE/FV_{h_1}}$ are constructed using a second-level agglomeration generated by applying recursive agglomerations [6, 19].

Remark It is noted here that by taking the quantity $[\mathcal{C}'\triangle_l'^2]$ out of the integration operators in Eq. (14), a mathematical inconsistency similar to that described in [25] is introduced. In the variational context, this inconsistency can be overcome, if desired, by a global minimization procedure that is described in Appendix A of this paper. However for practical purposes — mainly, in order to reduce computational overhead — the consistent procedure for computing $[\mathcal{C}'\triangle_l'^2]$ was not adopted for generating the numerical results discussed in this paper.

5 Numerical solution

The static and dynamic versions of the VMS-LES method presented in the previous sections were implemented in the AERO-F module of the nonlinear aeroelastic simulation platform AERO-F [26, 27]. AERO-F is a domain-decomposition-based, massively parallel, unstructured, three-dimensional, Navier-Stokes compressible flow solver with built in moving mesh capabilities. It blends an upwind scheme for the convective fluxes based on Roe's [28] approximate Riemann solver with a P1 finite element Galerkin approximation of the diffusive fluxes and source terms. Higher-order spatial accuracy is achieved through the use of a multidimensional piecewise linear reconstruction [29] that follows the principle of the Monotonic Upwind Scheme for Conservative Laws (MUSCL) [30]. Stabilization is obtained by a numerical diffusion that is based on sixth-order derivatives [31]. The associated numerical dissipation has a localized effect on high frequencies, which reduces its interaction with subgrid-scale modeling in turbulent flow simulations. Within this fluid module, RANS, LES and Hybrid turbulence models can be coupled with Reichardt's wall function [32]. AERO-F has the capability of performing time-integration with a three-point backward-difference *implicit* scheme as well as a fourth-order Runge-Kutta *explicit* scheme. In the low speed limit, it resorts to Roe-Turkel preconditioning of dissipation terms [33, 34] to overcome the numerical difficulties that are usually encountered by compressible flow solvers.

6 VMS-LES of turbulent flows on moving grids

The static and dynamic versions of the VMS-LES method for moving grids presented in the previous sections are applied to heaving and pitching of a NACA-0012 extruded airfoil. These flow configurations are useful in the anal-

ysis and design of MAV wing sections. All simulations presented in this section utilize an arbitrary Lagrangian/Eulerian form of Reichardt's wall law [35] and an implicit second-order time-stepping scheme that is provable second-order time-accurate on moving meshes and obeys its discrete geometric conservation law (DGCL) [36]. The results obtained using the VMS-LES methods are also compared with the classical constant coefficient Smagorinsky LES model [11] (Smag LES), the classical Favre averaged Germano dynamic LES model [13,37] (dynamic LES) and to experimental data wherever possible.

6.1 VMS-LES simulation of the Knoller-Betz effect

The Knoller-Betz effect symbolizes the ability of sinusoidally plunging airfoil to produce thrust. This is an important consideration for the design of propulsion systems of MAVs due to the excessive weight associated with traditional battery driven fixed wing propulsive systems. Various experimental and numerical investigations of this phenomenon have been carried out over the years to understand the evolution of thrust indicative wake structures [38]. It was observed both numerically and experimentally in [38] that the wake patterns at Strouhal numbers greater than 1.0 were non-symmetric, indicating that viscous effects/flow separation may be important in understanding the wake evolution. This sub-section delves into the study qualitatively the evolution of these wake structures using the static VMS-LES method.

To this end, a qualitative simulation of a plunging extruded NACA-0012 airfoil at a Reynolds number of $61,000$ based on the chord length of $1.22m$ is performed here. The airfoil is plunged with a reduced frequency of $k = 12.3$ and a non-dimensional plunge amplitude of $h = 0.12$ (resulting in a Strouhal number of 1.476). The computational domain is delimited by a circular cylinder of diameter $20c_r$. Symmetric boundary conditions are imposed at the two wing tips. The mesh has $14,450,920$ tetrahedra and $2,516,690$ nodes. Preferential mesh refinement is introduced in the regions of the separated wake as shown in Fig. 2.

As seen in Fig. 3 the final wake pattern shows the dual mode vortex street as observed in [38], which is indicative of thrust and lift as seen in the plot of averaged lift and drag (Fig. 4).

6.2 VMS-LES simulation of the dynamic stall of a NACA-0012 extruded airfoil

Many low speed aerodynamics applications involve highly unsteady hovering flight regimes that call for the delay of aerodynamic stall. Dynamic stall is

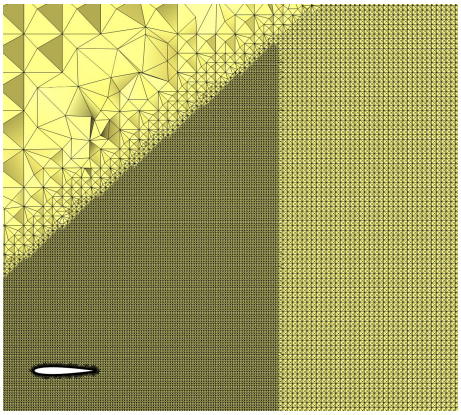

Fig. 2. Preferential refinement in the wake of the the NACA-0012 airfoil

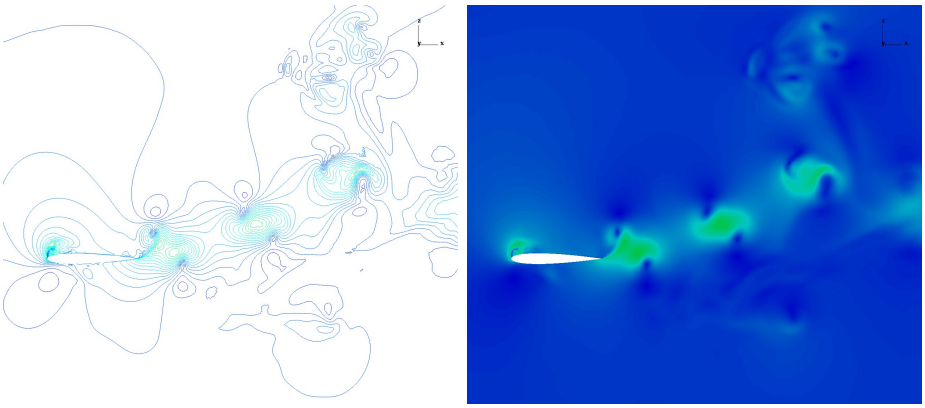

Fig. 3. (left) Contour plots and (right) wake pattern showing the dual-mode vortex street of the plunging NACA-0012 airfoil using VMS-LES method

an unsteady phenomenon where pitching a wing beyond its static stall angle results in maximum values of lift, drag and moment coefficients that far exceed those achieved in the static case. This phenomenon is characterized by a massive flow separation and a reattachment process that results in a highly nonlinear hysteresis.

In order to test the performance of the different LES models at predicting large scale unsteady effects and to gain insight into the phenomenon of dynamic stall, the flow over a pitching NACA-0012 wing in deep stall regime is pursued here. The obtained numerical results are compared to the experimental data reported in [39]. The considered unswept wing section has a span of $1m$ and a chord length (c_r) of $1.22m$. It is sinusoidally pitched about the quarter chord so that the angle of attack is varied as $\alpha = 15° + 10° sin(\omega t)$ where ω is chosen so that the reduced frequency is $k = \omega \times c_r/U_\infty = 0.15$, with U_∞ being the free-stream velocity. The free-stream Mach number is set to $M_\infty = 0.09$ and the Reynolds number based on the chord length is set to $Re = 2.6 \times 10^6$.

The computational domain is delimited by a circular cylinder of diameter $20c_r$. Symmetric boundary conditions are imposed at the two wing tips. The mesh

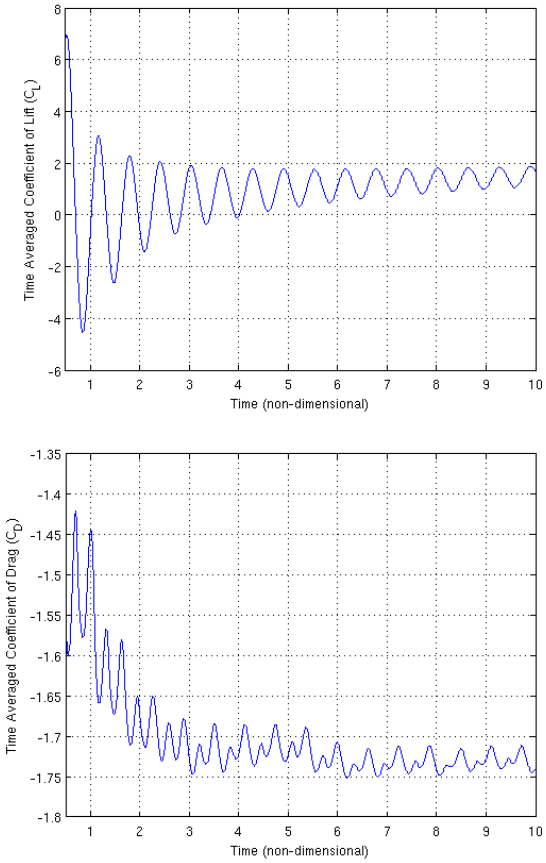

Fig. 4. (top) Time averaged lift and (right) time averaged drag of the plunging NACA-0012 extruded airfoil using VMS-LES method

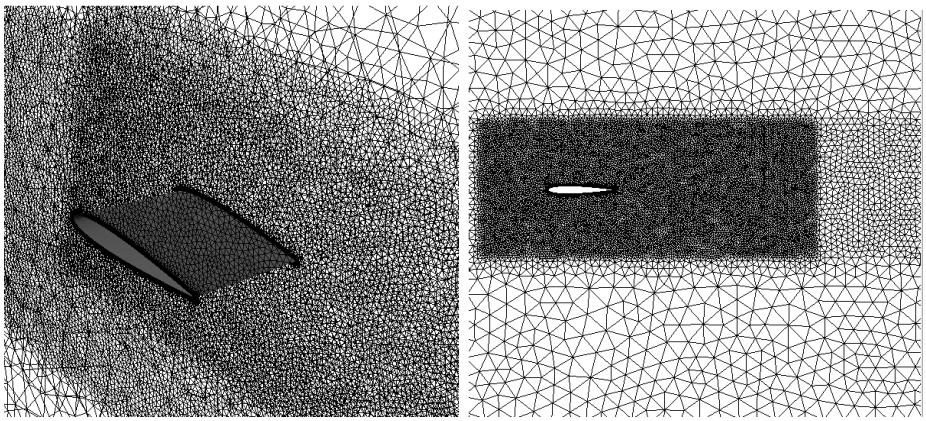

Fig. 5. Pitching NACA-0012 wing section: computational domain and mesh details

has $8,557,236$ tetrahedra and $1,504,611$ nodes. Preferential mesh refinement is introduced in the regions of the separated wake as shown in Fig. 5. For this flow, the estimated Taylor microscale is $\lambda \approx 2.98 \times 10^{-3} m$, the estimated Kolmogorov microscale is $\eta \approx 1.94 \times 10^{-5} m$ and the estimated Kolmogorov time scale is $\tau \approx 2.6 \times 10^{-5} s$. The characteristic length of the smallest grid

spacing near the wing and the largest grid spacing in the far field are $2.0 \times 10^{-4}m$ and $9.2 \times 10^{-2}m$, respectively. The time-step for the simulation was set to $\Delta t = 2 \times 10^{-4}s$.

The number of layers is set to one in the first- and second-level agglomerations and the depth of the second-level agglomeration is set to one for the dynamic VMS-LES. The lift and pitching moment hysteresis loops for the deep stall considered here is then computed using the four different LES models, namely the Smag LES, dynamic LES, VMS-LES and dynamic VMS-LES. These loops are plotted in Figs. 6, 7 along with the experimental data reported in [39]. It is observed that while all LES models deliver good lift hysteresis predictions, the dynamic VMS-LES model delivers the best predictions for the pitching moment coefficient. Furthermore, it is noted that the dynamic form of VMS-LES significantly improves the performance of its static counterpart in the prediction of hysterisis.

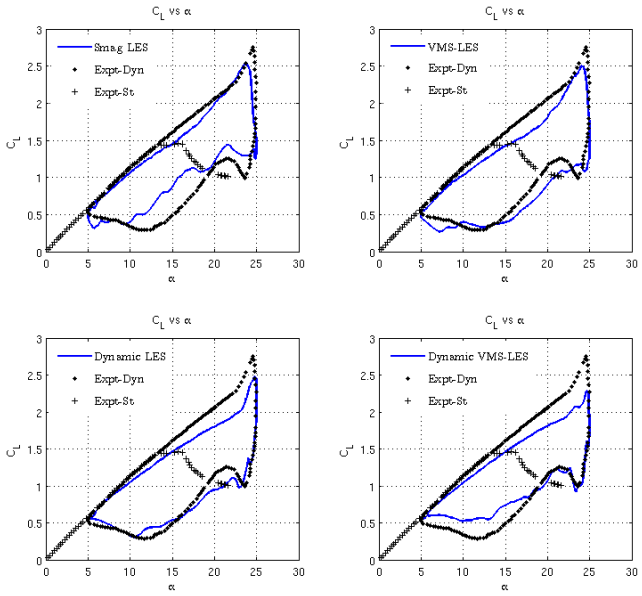

Fig. 6. Pitching NACA-0012 wing section: lift coefficients

7 Conclusions

The static and dynamic VMS-LES method developed in [5, 6] has been applied to simulate the Knoller-Betz effect of a heaving airfoil and to simulate the dynamic stall of a pitching airfoil. The obtained numerical results suggest the superior performance of VMS-LES as a viable LES model for applications that involve turbulent flow computations over moving/deforming objects. The obtained numerical results for the dynamic stall of the pitching airfoil suggest

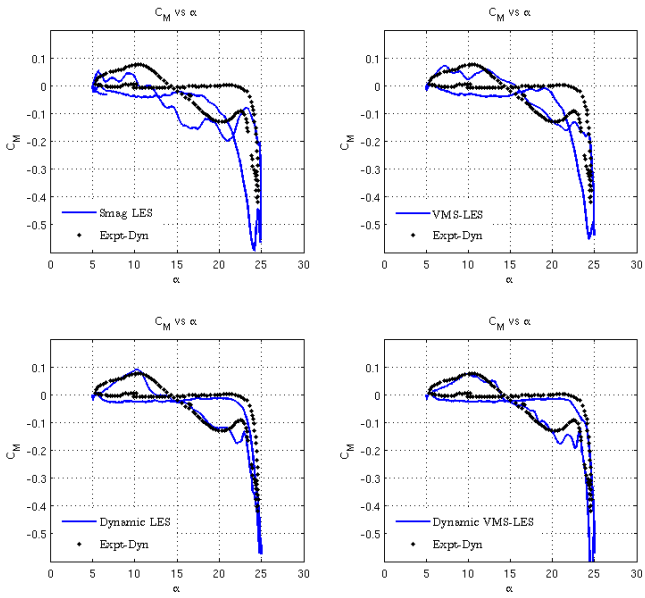

Fig. 7. Pitching NACA-0012 wing section: moment coefficients

that this dynamic VMS-LES method tends to deliver more accurate results than the static VMS-LES and the classical LES and dynamic LES methods. In particular, it is found that the dynamic VMS-LES method significantly improves the performance of its static counterpart for the prediction of lift/drag/moment characteristics.

Predicting accurate space-time correlation is an important feature that LES turbulence models need to satisfy. The dynamic version of the VMS-LES method developed here is an attempt to bring in the effect of time correlations into LES simulation, and hence it would be important to study if this model gives good space-time correlation. It would also be of interest to study turbulent flow simulations using the VMS-LES method to characterize the flow over flexible structures, there by working in the full realm of fluid-structure interaction.

Acknowledgments

Both authors acknowledge the partial support and computing time from the Army High Performance Computing Research Center and the Air Force Office of Scientific Research under Grant F49620-01-1-0129. The authors also thank the computer time provided by NSF MRI Grant #CNS–0421498, NSF MRI Grant #CNS–0420873, NSF MRI Grant #CNS–0420985, NSF sponsorship of the National Center for Atmospheric Research, the University of Colorado, and a grant from the IBM Shared University Research (SUR) program. The

first author is extremely indebted and thankful to Dr. Charbel Bou Mosleh for creating all the meshes involved in this paper and for his invaluable advices at each stage of this work. The first author is also thankful to Prof. Bruno Koobus for his constant supervision and help during the course of this work.

Appendix A - A Consistent method for computing $\mathcal{C}'\triangle_l'^2$

A consistent procedure for determining the quantity $\mathcal{C}'\triangle_l'^2$ from the first of Eqs. (14) is detailed in this paragraph. The error in satisfying Eqs. (14) for a given coefficient field $\mathcal{C}'\triangle_l'^2$ is given by

$$\mathbf{E}_i = \mathbf{R}_i - \mathbf{M}_S\Big(\Phi'_{i_{h_1}}, \mathbf{W}'_{h_1}, \mathcal{C}'\triangle_l'^2\Big) + \mathbf{M}_S\Big(\Phi'_{i_{h_{2,1}}}, \mathbf{W}'_{h_{2,1}}, (\frac{\triangle'_{h_2}}{\triangle'_{h_1}})^2\mathcal{C}'\triangle_l'^2\Big) \tag{16}$$

where,

$$\mathbf{R}_i = \mathbf{B}(\mathcal{X}_{i_{h_{2,1}}}, \Phi_{i_{h_{2,1}}}, \mathbf{W}_{h_{2,1}}) - \mathbf{B}(\mathcal{X}_{i_{h_1}}, \Phi_{i_{h_1}}, \mathbf{W}_{h_1}) \tag{17}$$

Hence, the function $\mathcal{C}'\triangle_l'^2$ that best satisfies the integral equations in Eq. (16) can be evaluated as

$$\mathcal{C}'\triangle_l'^2 = \arg\min_{\mathcal{C}'\triangle_l'^2 \in X} J(\mathcal{C}'\triangle_l'^2) \tag{18}$$

where,

$$J(\mathcal{C}'\triangle_l'^2) = \int_\Omega \mathbf{E}_i^T\mathbf{E}_i d\Omega \tag{19}$$

is a functional of $\mathcal{C}'\triangle_l'^2$ and the integral extends over the fluid domain Ω and the space of solutions X is given by

$$X = \{\mathcal{C}'\triangle_l'^2 : \mathcal{C}'\triangle_l'^2 \in \mathcal{H}_0^0\} \tag{20}$$

Denoting $\mathcal{C}'\triangle_l'^2$ by $\mathfrak{C}$, and setting variation of $J(\mathfrak{C})$ to zero the following variational equation is obtained

$$\delta J(\mathfrak{C}) = 2\int_\Omega \mathbf{E}_i^T\delta\mathbf{E}_i d\Omega = 0 \tag{21}$$

and therefore

$$\begin{aligned}\int_\Omega \Big[\mathbf{R} - \mathbf{M}_S\Big(\Phi'_{i_{h_1}}, \mathbf{W}'_{h_1}, \mathfrak{C}\Big) + \mathbf{M}_S\Big(\Phi'_{i_{h_{2,1}}}, \mathbf{W}'_{h_{2,1}}, (\frac{\triangle'_{h_2}}{\triangle'_{h_1}})^2\mathfrak{C}\Big)\Big]^T \\ \Big[-\mathbf{M}_S\Big(\Phi'_{i_{h_1}}, \mathbf{W}'_{h_1}, \delta\mathfrak{C}\Big) + \mathbf{M}_S\Big(\Phi'_{i_{h_{2,1}}}, \mathbf{W}'_{h_{2,1}}, (\frac{\triangle'_{h_2}}{\triangle'_{h_1}})^2\delta\mathfrak{C}\Big)\Big]d\Omega = 0\end{aligned} \tag{22}$$

which can be rearranged as

$$\int_\Omega \Big[\mathbf{M}_S\Big(\Phi'_{i_{h_1}}, \mathbf{W}'_{h_1}, \mathfrak{C}\Big)\mathbf{M}_S\Big(\Phi'_{i_{h_1}}, \mathbf{W}'_{h_1}, \delta\mathfrak{C}\Big) + \mathbf{M}_S\Big(\Phi'_{i_{h_{2,1}}}, \mathbf{W}'_{h_{2,1}}, (\frac{\triangle'_{h_2}}{\triangle'_{h_1}})^2\mathfrak{C}\Big)$$
$$\mathbf{M}_S\Big(\Phi'_{i_{h_{2,1}}}, \mathbf{W}'_{h_{2,1}}, (\frac{\triangle'_{h_2}}{\triangle'_{h_1}})^2\delta\mathfrak{C}\Big) - \mathbf{M}_S\Big(\Phi'_{i_{h_1}}, \mathbf{W}'_{h_1}, \mathfrak{C}\Big)\mathbf{M}_S\Big(\Phi'_{i_{h_{2,1}}}, \mathbf{W}'_{h_{2,1}}, (\frac{\triangle'_{h_2}}{\triangle'_{h_1}})^2\delta\mathfrak{C}\Big)$$
$$-\mathbf{M}_S\Big(\Phi'_{i_{h_{2,1}}}, \mathbf{W}'_{h_{2,1}}, (\frac{\triangle'_{h_2}}{\triangle'_{h_1}})^2\mathfrak{C}\Big)\mathbf{M}_S\Big(\Phi'_{i_{h_1}}, \mathbf{W}'_{h_1}, \delta\mathfrak{C}\Big)\Big]d\Omega =$$
$$\int_\Omega R\Big[\mathbf{M}_S\Big(\Phi'_{i_{h_1}}, \mathbf{W}'_{h_1}, \delta\mathfrak{C}\Big) - \mathbf{M}_S\Big(\Phi'_{i_{h_{2,1}}}, \mathbf{W}'_{h_{2,1}}, (\frac{\triangle'_{h_2}}{\triangle'_{h_1}})^2\delta\mathfrak{C}\Big)\Big]d\Omega \tag{23}$$

By choosing an appropriate discrete representation for $\mathfrak{C}$, for example, $\mathfrak{C} = \sum_{i=1}^{N} \mathfrak{C}_i\varphi_i$ and choosing $\delta\mathfrak{C}_i = \varphi_i$, one can obtain a Galerkin discretization for Eq. (23) and solve the resulting global system of equations to obtain the coefficients $\mathfrak{C}_i$.

References

[1] Hughes TJR, Mazzei L, Jansen KE. Large eddy simulation and the variational multiscale method, Comput. Vis. Sci. 2000; 3-47.

[2] Hughes TJR, Mazzei L, Oberai AA, Wray AA. The multiscale formulation of large eddy simulation: decay of homogeneous isotropic turbulence, Phys. Fluids 2001; 13:505-512.

[3] Hughes TJR, Oberai AA , Mazzei L. Large eddy simulation of turbulent channel flows by the variational multiscale method, Phys. Fluids 2001; 13:1784-1799.

[4] Collis SS, Monitoring unresolved scales in multiscale turbulence modeling, Phys. Fluids 2001; 1800-1806.

[5] Koobus B, Farhat C. A variational multiscale method for the large eddy simulation of compressible turbulent flows on unstructured meshes - application to vortex shedding, Comput. Meths. Appl. Mech. Engrg. 2004; 193:1367-1384.

[6] Farhat C, Rajasekharan A, Koobus B. A dynamic variational multiscale method for large eddy simulations on unstructured meshes, Comput. Meths. Appl. Mech. Engrg. 2006; 195:1667-1691.

[7] Rajasekharan A, Farhat C, Bou-Mosleh C. Application of a dynamic variational multiscale method to the LES of separated turbulent flows, AIAA Paper 2007-726, 2007.

[8] Ramakrishnan S, Collis SS. Variational multiscale modeling for turbulence control, *First Flow Control Conference*, AIAA 2002-3280, 2002.

[9] Calo VM. Residual-based multiscale turbulence modeling, finite volume simulations of bypass transition, PhD. Dissertation, Stanford University, 2004.

[10] Jansen KE, Tejada-Martínez AE. An evaluation of the hierarchical basis in variational multiscale LES, AIAA Paper No. 2002-0283, 2002.

[11] Smagorinsky J. General circulation experiments with the primitive equations, Mon. Weather Rev. 1963; 91:99-164.

[12] Holmen J, Hughes TJR, Oberai AA, Wells GN. Sensitivity of the scale partition for variational multiscale LES of channel flow, Phys. Fluids 2004; 16(3):824-827.

[13] Germano M, Piomelli U, Moin P, Cabot WH. A dynamic subgrid-scale eddy viscosity model, Phys. Fluids 1991; A3:1760-1765.

[14] Gravemeier V, Wall WA, Ramm E. A three level finite element method for the instationary incompressible Navier-Stokes equations, Comput. Meths. Appl. Mech. Engrg. 2004; 193:1323-1366.

[15] Franca L, Farhat C, Lesoinne M, Russo A. Unusual stabilized finite element methods and residual-free bubbles, Internat. J. Numer. Meths. Fluids 1998; 27:159-168.

[16] Oberai AA, Wanderer J. A dynamic approach for evaluating parameters in a numerical method, Internt. J. Numer. Meths. Engrg. 2005; 62:50-71.

[17] Oberai AA, Wanderer J. Variational formulation of the germano identity for the navier-stokes equations, J. Turb. 2005; 6:1-17.

[18] Morinishi Y, Vasilyev OV. Vector level identity for dynamic subgrid scale modeling in large eddy simulation, Phys. Fluids 2002; 14:3616-3623.

[19] Rajasekharan A. Variationally consistent multiscale formulations and ALE time integrators for Large Eddy Simulation of turbulent flows on dynamic grids, PhD. Dissertation, Stanford University, 2008.

[20] Lallemand MH, Steve H, Dervieux A. Unstructured multigridding by volume agglomeration: current status, Comput. & Fluids 1992; 21:397-433.

[21] Gravemier V. Scale-separating operators for variational multiscale large eddy simulation of turbulent flows, J. Comp. Phys. 2006; 212:400-435.

[22] Mallat S. A wavelet tour of signal processing, Academic Press, 1999.

[23] Dubois T, Jauberteau F, Temam R. Dynamic multilevel methods and the numerical simulation of turbulence, Cambridge University Press, 1999.

[24] Sagaut P. Large eddy simulation for incompressible flows, Third Edition, Springer-Verlag, 2006.

[25] Ghosal S., Lund TS, Moin P, Akselvoll K. A dynamic localization model for large-eddy simulation of turbulent flows, J. Fluid Mech., 1995; 286:229-255.

[26] Farhat C, Geuzaine P, Brown G. Application of a three-field nonlinear fluid-structure formulation to the prediction of the aeroelastic parameters of an F-16 fighter, Comput. & Fluids 2003; 32:3-29.

[27] Geuzaine P, Brown G, Harris C, Farhat C. Aeroelastic dynamic analysis of a full F-16 configuration for various flight conditions, AIAA J. 2003; 41:363-371.

[28] Roe PL. Approximate Riemann solver, parameters vectors and difference schemes, J. Comp. Phys. 1981; 43:357-371.

[29] Dervieux A. Steady Euler simulations using unstructured meshes, Von Kármán Institute Lecture Series, 1985.

[30] Van Leer B. Towards the ultimate conservative difference scheme V: a second-order sequel to Godunov's method, J. Comp. Phys. 1979; 32:361-370.

[31] Debiez C, Dervieux A. Mixed element volume MUSCL methods with weak viscosity for steady and unsteady flow calculation, Comput. & Fluids 1999, 29:89-118.

[32] Hinze JO. Turbulence, McGraw-Hill, NewYork, 1959.

[33] Turkel E. Preconditionned methods for solving the incompressible and low-speed compressible equations, J. Comp. Phys. 1987; 72:277-298.

[34] Viozat C. Implicit upwind schemes for low Mach number compressible flows, INRIA Report N0. 3084, January 1997.

[35] Tran H, Koobus B, Farhat C. Numerical solution of vortex dominated flow problems with moving grids, AIAA Paper 98-0766, 1998.

[36] Geuzaine P, Grandmont C, Farhat C. Design and analysis of ALE schemes with provable second-order accuracy for inviscid and viscous flow simulations, J. Comp. Phys. 2003; 191:206-227.

[37] Camarri S, Salvetti MV, Koobus B, Dervieux A. Large-eddy simulation of a bluff body flow on unstructured grids, Int. J. Numer. Meths. Fluids 2002; 40:1431-1460.

[38] Jones KD, Dohring CM, Platzer MF. Experimental and computational investigation of the Knoller-Betz effect AIAA J. 1998; 36(7):1240-1246.

[39] McCroskey WJ, Carr LW, McAlister KW. Dynamic stall experiments on oscillating airfoils, AIAA J. 1976; 14:57-63.